

Original Article

An MRI radiomics nomogram improves the accuracy in identifying eligible candidates for fertility-preserving treatment in endometrioid adenocarcinoma

Bi-Cong Yan^{1,2*}, Feng-Hua Ma^{3*}, Ying Li^{2*}, Yan-Feng Fan¹, Zhi-Long Huang¹, Xiao-Liang Ma^{2,3}, Xue-Ting Wen², Jin-Wei Qiang²

¹Department of Diagnostic and Interventional Radiology, Shanghai Jiaotong University Affiliated Sixth People's Hospital, 600 Yi Shan Road, Shanghai 200233, China; ²Department of Radiology, Jinshan Hospital, Fudan University, 1508 Longhang Road, Shanghai 201508, China; ³Department of Radiology, Obstetrics & Gynecology Hospital, Fudan University, 128 ShenYang Road, Shanghai 200090, China. *Equal contributors.

Received October 13, 2021; Accepted February 18, 2022; Epub March 15, 2022; Published March 30, 2022

Abstract: It is difficult to identify eligible candidates for fertility-preserving treatment (FPT) among endometrioid adenocarcinoma (EAC) and atypical hyperplasia (AH) patients. Therefore, new approaches for improving the accuracy of candidate selection are warranted. From December 2014 to January 2020, 236 EAC/AH patients (age <50 and premenopausal) were retrospectively reviewed and randomly divided into the primary group (n=158) and validation group 1 (n=78). From February 2020 to December 2021, 51 EAC/AH patients were prospectively enrolled and formed the validation group 2. From the primary group, 385 features were extracted using pyradiomics from multiparameter magnetic resonance imaging (MRI) (including T2-weighted imaging, diffusion-weighted imaging, apparent diffusion coefficient, and contrast enhancement sequences) and 13 radiomics features were selected using a least absolute shrinkage and selection operator. A clinical model based on clinical information (myometrial invasion on MRI and tumor grade in curettage) and a radiomics nomogram by integrating clinical information with the radiomics features was developed to identify eligible candidates of FPT. For identifying eligible candidates of FPT, the areas under the receiver operating characteristic curve (AUCs) were 0.63 (95% confidence interval [CI]: 0.53-0.73) in the primary group, and 0.62 (95% CI: 0.45-0.78) and 0.69 (95% CI: 0.53-0.86) in validation groups 1 and 2, respectively, for the clinical model; were 0.86 (95% CI: 0.80-0.93) in the primary group, and 0.82 (95% CI: 0.71-0.93) and 0.94 (95% CI: 0.87-1.0) in validation groups 1 and 2, respectively, for the radiomics nomogram. With the help of radiomics nomogram, the treatment decision determined from the clinical model was revised in 45 EAC/AH patients. The net reclassification index (NRI) was 0.80 and integrated discrimination improvement (IDI) was 0.17, indicating that the nomogram could improve the accuracy in identifying eligible EAC/AH candidates for FPT.

Keywords: Endometrioid carcinoma, fertility preservation, radiomics, nomogram, magnetic resonance imaging

Introduction

Endometrial cancer (EC) is becoming one of the most common gynecologic malignancies, demonstrating increasing morbidity [1, 2]. In a population-based registry (Geneva Cancer Registry), 18% of women younger than 45 years had early-stage EC at the time of final surgical pathology [1, 3]. Furthermore, approximately 57% of young EC patients are nulliparous at diagnosis, because of late childbearing and rising EC incidence rates [3]. The standard treatment for EC is total hysterectomy and bilateral

salpingo-oophorectomy, which leads to permanent loss of fertility for women of childbearing age. Therefore, there is an urgent need for conservative, non-surgical treatment approaches. For young patients who want to preserve reproductive ability, progestin-based treatments combined with delaying surgery can be administered in those with endometrium-confined grade I endometrioid adenocarcinoma (EAC) (i.e., the absence of myometrial invasion [non-MI], cervical stromal invasion [CSI], and extrauterine metastasis [EM], including ovarian metastasis and lymph node metastasis) or

Radiomics nomogram in endometrioid carcinoma treatment

atypical hyperplasia (AH) [4]. However, a prerequisite for this conservative non-surgical treatment is a precise preoperative evaluation.

Dilatation and curettage (D&C) is recommended for evaluate the tumor grade of EC, however, the findings are frequently discordant with those at final surgical pathology [5-8]. Helpman et al. reported that 22% of grade I ECs diagnosed by biopsy were upgraded to grade II or III based on the surgical pathology [8].

Magnetic resonance imaging (MRI) may be the preferred modality for evaluating the presence of MI. However, previous studies have reported varying accuracies [9-11]. One recent study showed that the accuracy and the areas under the curve (AUC) for MI were only 63% and 0.75, respectively, and that MRI produced a false-negative result in approximately 50% of patients. Misjudgments tended to occur for patients with superficial MI [12], and MRI assessed MI in premenopausal women with grade (G) 1 EC had an accuracy of 63%, sensitivity of 42%, specificity of 85%, and AUC of 0.75, respectively [13]. Another recent study showed that the tumor apparent diffusion coefficient (ADC) value was associated with pathologic upgrading for biopsy-proven grade I ECs [14]. However, whether the ADC can be used to assess the aggressiveness of EC remains controversial. The results from D&C and MRI suggest that decisions based on conventional MRI sequences (such as T2WI) and clinical information are imprecise in identifying eligible candidates for FPT.

The radiomics-based nomogram is a useful tool that has been widely applied in different field of oncology [15]. By integrating clinical and imaging information, the nomogram plays an important role in the drive towards personalized medicine and helps clinicians in treatment planning [16]. However, no studies have used radiomics nomograms to help gynecologists assess EC patients for receiving FPT. Therefore, we hypothesized that tumor radiomics has potential as a supplementary imaging biomarker for preoperatively assessing pathological tumor grade and MI in EC. In this study, we developed an MRI radiomics nomogram to identify eligible candidates for FPT among EAC/AH patients.

Materials and methods

Patients

The Institutional Review Board approved this study, and informed consent was waived for

retrospective patients and obtained for prospective patients (approval number: 2020-10). All patients were collected from Obstetrics & Gynecology Hospital of Fudan University. From December 2014 to January 2020, the electronic medical records of a total of 297 consecutive pathologically proven EAC/AH patients were reviewed. Potential candidates for FPT met the following criteria: 1) age younger than 50 years and premenopausal status; 2) total hysterectomy and a diagnosis of EAC/AH; 3) a lack of other reproductive system malignant tumors, or other progesterin-dependent cancers, such as breast or ovarian cancer; and 4) MRI scanning with T1-weighted imaging (T1WI), T2-weighted imaging (T2WI) with fat saturation (FS), contrast-enhanced (CE)-T1WI with FS, diffusion-weighted imaging (DWI) and ADC sequences. The exclusion criteria were as follows: 1) radiotherapy, chemotherapy, and hormone-based treatment administered before surgery (n=10); 2) absence of preoperative pelvic MRI (n=15); 3) insufficient imaging quality for analysis owing to motion artifacts, or inability to see the tumor on MRI (n=27); and 4) a non-EAC pathologic diagnosis (n=9). Finally, a total of 236 patients with 232 EACs and four AHs (mean age 42±6.1 years) were enrolled as potential candidates for FPT. The 236 patients were randomly divided into the primary group and the validation group 1 according to a ratio of 2 to 1. Furthermore, from February 2020 to December 2021, 67 eligible patients for FPT were prospectively enrolled, and 51 patients were finally included and formed the validation group 2. In addition to retrospective inclusion and exclusion criteria, we also included the EAC/AH patients confirmed by D&C rather than hysterectomy, who had strong desire to preserve fertility and followed-up more than 3 months, and additionally excluded the patients who withdrew FPT within 3 months.

General clinical information from each patient was collected, including age, cancer antigen 125 (CA125) level, oestrogen receptor (ER) level, progesterone receptor (PR) level and p53 level, etc. The CA125 level was measured within 1 week before the surgery using chemiluminescence approach (Abbott Laboratories, US). And these clinical information were analyzed to select FPT independent factors by multivariable logistic regression based on the data of the primary group.

Eligible candidates for FPT were defined as those with: 1) pathologically proven grade I

Radiomics nomogram in endometrioid carcinoma treatment

Table 1. MRI sequences and parameters in endometrial cancer patients

Sequences	TR/TE (ms)	NEX	AT (s)	Matrix	FOV (mm)	Slice thickness/gap (mm)
Axial T1WI	761/10	1	46	512×512	380	4/1
Axial T2WI-FS	4000/98	1	146	512×512	370	4/1
DWI (b=0, 1000 s/mm ²)	4000/100	5	98	256×256	300	5/1
Axial CE-T1WI-FS	196/2.9	2	172	512×512	400	4/1

AT, acquisition time; CE-T1WI, contrast-enhanced T1WI; DWI, diffusion-weighted imaging; FS, fat saturation; NEX, number of excitation; T1WI, T1-weighted imaging; T2WI, T2-weighted imaging; TE, time of echo; TR, time of repetition.

EAC, or AH, and 2) a pathologically proven endometrium-confined tumor (absence of MI, CSI, EM) [4, 17, 18]. Other EC patients were defined as non-FPT.

Imaging

All enrolled patients received pelvic MRI within 30 days before surgery. The mean interval between MRI and surgery was 20 days (range, 5-30 days). MRI was performed using a 1.5-T scanner (Avanto; Siemens, Germany) with an eight-channel pelvic phased-array coils. The patients laid in a supine position and breathed freely during the acquisition. MRI was performed by referring to the European Society of Urogenital Radiology guidelines. The sequences and parameters are shown in **Table 1**. CE-T1WI with FS at the arterial, venous and delay phases was performed immediately and 90-120 s and 150-180 s after the intravenous administration of gadopentetate dimeglumine at a dose of 0.2 mmol/kg of body weight and a rate of 2 to 3 ml/s. The ADC map was automatically generated based on DWI sequences (b=0 and b=1000 s/mm²).

MRI evaluation of EC and myometrial invasion

All MRI data (including the five sequences) were reviewed independently by radiologists 1 and 2 (with five and 13 years of experience in gynecologic imaging, respectively) who were blind to the results of the D&C and surgical pathology. All surgical pathological diagnoses were made by attending pathologists with over 15 years of experience in gynecologic pathology. Any disagreement was solved by consensus.

EC was determined as a focal endometrial lesion with slightly lower signal intensity (SI) than the normal endometrium on T2WI, a higher SI on DWI and lower SI on the corresponding ADC maps and milder enhancement on CE-T1WI, comparing the normal myometrium.

Tumor size was defined as the maximum tumor diameter measured retrospectively on T2WI. MI was evaluated as non-MI, or the presence of MI (including superficial MI [SMI: 0< MI <50%] and deep MI [DMI: MI ≥50%]). A sign of disconnection of the junctional zone on T2WI, or subendometrial enhancement line on CE-T1WI was considered the presence of MI. CSI and EM were diagnosed according to a previous study [19].

Radiomics features extraction and selection

The patients' images were first imported into the medical imaging software MitkWorkbench ([http://mitk.org/wiki/The_Medical_Imaging_Interaction_Toolkit_\(MITK\)](http://mitk.org/wiki/The_Medical_Imaging_Interaction_Toolkit_(MITK))). Axial DWI, ADC map, and CE-T1WI (delayed phase) were aligned to axial T2WI. Regions of interest (ROIs) were manually drawn along the tumor margin on each slice of the T2WI by radiologist 1 (B.C.Y) while referencing the DWI, ADC map and CE-T1WI. The ROIs were mapped to all remaining sequences. The ROIs of each patient were drawn a second time by radiologist 1 one month later and by radiologist 2 (Y.L). After tumor segmentation, the merged 3D strategy was used to extract radiomics features from the ROIs delineated by radiologist 1 by using pyradiomics (<https://pypi.org/project/pyradiomic/>). To ensure comparability of the MRI grey values, imaging preprocessing was performed. A fixed bin width of 1 was used to compute radiomics features. All radiomics feature implementations followed the IBSI recommendation (<https://arxiv.org/abs/1612.07003>).

The inter- and intraclass correlation coefficients (ICCs) of the extracted features were calculated to assess the stability of the radiomics features. Features with both inter- and intraclass coefficients larger than 0.90 were considered robust and reproducible. Pearson's correlation was used to identify redundant features. If two features had a Pearson correlation coefficient > 0.9, the feature with the larger mean abso-

Radiomics nomogram in endometrioid carcinoma treatment

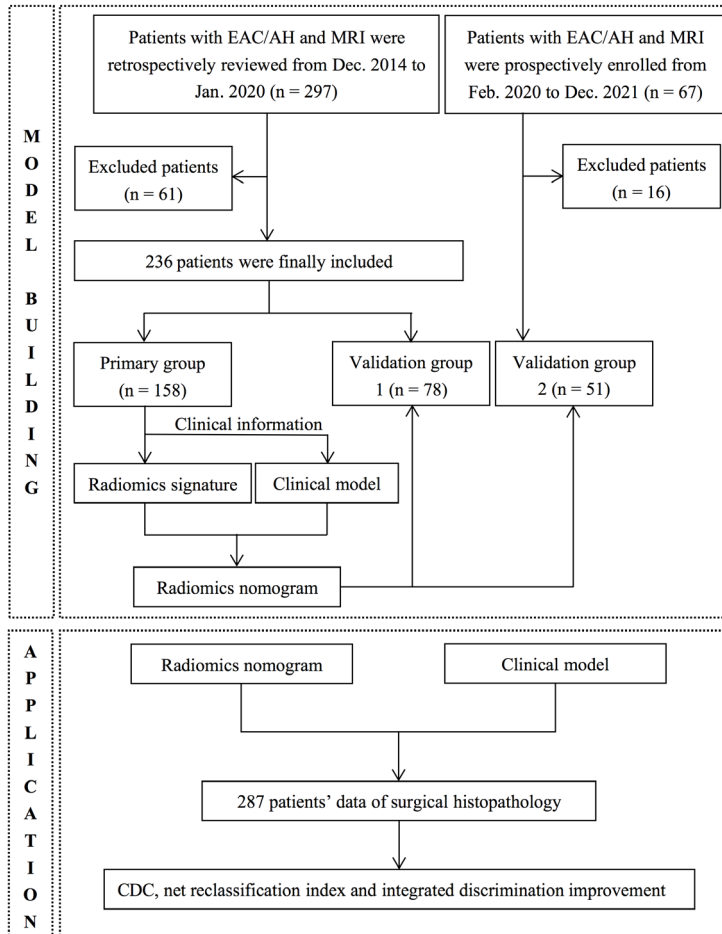


Figure 1. The workflow of the study. AH, atypical hyperplasia; CDC, clinical decision curve; EAC, endometrioid adenocarcinoma.

lute coefficient was removed. Then, the least absolute shrinkage and selection operator (LASSO) was used to select features associated with eligible candidates for FPT with 10-fold cross-validation to avoid overfitting [20]. A radiomics score (Radscore) was produced by linear fitting of the selected features.

Clinical and radiomics nomogram models development

The histology subtype and grade of each tumor in the D&C reports and in the final pathologic reports of total hysterectomy were reviewed. The tumor stage was determined according to the International Federation of Gynecology and Obstetrics (FIGO) grading system based on the final pathologic reports.

A clinical model simulating clinical practice for identifying eligible FPT candidates was devel-

oped by combining the MI status on MRI (0= non-MI and 1= MI [SMI and DMI]) and tumor grade in the curettage pathology (0= G1/AH and 1= G2-3 EAC) using linear logistic regression. The radiomics nomogram was developed by integrating multiparametric MRI (mpMRI) radiomics features with clinical information by using a multivariable logistic regression method based on the data of the primary group. The clinical model and the radiomics nomogram were also validated in the validation groups 1 and 2.

The areas under the receiver operating characteristic curve (AUCs) were used to evaluate the diagnostic performances of the radiomics nomogram and the clinical model for the primary and validation groups. The calibration curves were used to assess the goodness of fit of the radiomics nomogram. Clinical decision curve (CDC) analysis was performed to determine the radiomics nomogram's clinical usefulness and to quantify the net benefits at the threshold probabilities based on the whole dataset, i.e., the primary group,

the validation groups 1 and 2. The performances of the radiomics nomogram and the clinical model were compared using the net reclassification index (NRI) and total integrated discrimination index (IDI). The work flow of this study is shown in **Figure 1**.

Statistical analyses

The radscore, age, and CA125 were compared using an independent t-test after normality test; the findings on MRI, tumor grade in curettage pathology, and PR, ER and p53 status were compared using Pearson's chi-square test, or Fisher's exact test between FPT and non-FPT in the primary group and validation groups 1 and 2. All analyses were performed using R software (Version 3.6.1; <http://www.r-project.org/>). Statistical significance was defined as a two-sided *P*-value of less than 0.05. The "caret", "glmnet", "rms", "pROC",

Radiomics nomogram in endometrioid carcinoma treatment

Table 2. Clinicopathological characteristics of included EC patients in the primary and validation groups

Clinpathologic characteristics	Primary group (n=158)			Validation group 1 (n=78)			Validation group 2 (n=51)		
	Non-FPT (128)	FPT (30)	P value	Non-FPT (67)	FPT (11)	P value	Non-FPT (40)	FPT (11)	P value
Age (years)	42.7±5.8	41.8±6.7	0.05	42.9±5.1	39.8±8.8	0.08	43.4±6.8	40.5±6.7	0.43
CA125 (U/ml)	31.1±41.8	27.7±23.3	0.40	25.3±22.8	25.8±19.2	0.41	29.1±35.2	17.0±12.7	0.45
Tumor size (mm)	18.4±7.1	14.8±5.6	0.51	17.2±5.7	14.8±4.3	0.45	18.1±7.7	14.2±4.6	0.43
ER (-/+)	49/79	9/21	0.53	28/39	8/3	0.10	36/4	6/5	0.02
PR (-/+)	47/81	9/21	0.53	27/40	8/3	0.06	24/16	6/5	0.74
p53 (-/+)	69/59	17/13	0.84	37/30	10/1	0.04	32/8	6/5	0.12
CSI (-/+)	106/22	30/0	0.01	59/8	11/0	0.59	10/30	11/0	0.09
EM (-/+)	114/14	30/0	0.07	64/3	11/0	1.00	2/38	11/0	1.00
MI (non-MI/MI)	1/127	30/0	<0.001	1/66	11/0	<0.001	4/36	11/0	<0.001
RMI (non-MI/MI)	50/78	18/12	0.02	37/30	7/4	0.62	12/28	11/0	0.28
RCSI (-/+)	109/19	29/1	0.13	61/6	10/1	1.00	7/33	11/0	0.32
REM (-/+)	105/23	26/4	0.79	58/9	9/2	0.65	2/38	11/0	1.00
TGS (AH/G1/G2/G3)	0/86/34/8	3/27/0/0	<0.001	0/50/12/5	1/10/0/0	0.03	0/25/9/6	0/11/0/0	0.54
TGC (AH/G1/G2/G3)	6/96/10/16	3/27/0/0	0.09	0/49/8/10	1/10/0/0	0.05	0/23/12/5	1/10/0/0	0.02
FIGO (IA/IB/II-IV)	90/6/32	30/0/0	0.07	53/3/11	11/0/0/0	0.73	30/1/9	11/0/0	0.18
Radscore	0.1±0.2	0.4±0.2	0.51	0.1±0.1	0.2±0.1	0.04	0.1±0.2	0.6±0.3	0.43

AH, atypical hyperplasia; CA125, cancer antigen 125; CSI, cervical stromal invasion; DMI, deep myometrial invasion; EAC, endometrioid adenocarcinoma; EM, extrauterine metastasis; ER, estrogen receptor; FIGO, International Federation of Obstetrics and Gynecology; FPT, fertility-preserving treatment; LNM, lymph node metastasis; MI, myometrial invasion; OM, ovarian metastases; PR, progesterone receptor; RCSI, radiologist's assessment of cervical stromal invasion; REM, radiologist's assessment of extrauterine metastasis; RMI, radiologist's assessment of myometrial invasion; TGC, tumor grade in curettage; TGS, tumor grade in surgical pathology.

“dca.R” and “PredictABEL” packages were used in the analysis. DeLong's test was used to compare the performance between the radiomics nomogram and the clinical model.

Results

The clinicopathological characteristics of the included EAC/AH patients are summarized in **Table 2**. There were 209 G1 patients, 74 G2 and G3 patients, four AH patients who were diagnosed by surgical pathology. There were 225 patients staged as IA, and the remaining 62 patients were staged as higher stages. There were no significant differences in the levels of CA125 (P=0.97), ER (P=0.48), PR (P=0.17) or p53 (P=0.41) between the FPT and non-FPT patients by multivariable logistic regression (all P > 0.05). Surgical pathology confirmed that 52 patients were eligible FPT candidates and 235 patients were non-FPT patients (aged 40.1±7.4 years and 42.1±5.9 years, respectively, P=0.67). On MRI, the mean tumor sizes were 24.2±11.9 mm and 23.1±15.6 mm for the FPT and non-FPT patients, respectively (P=0.73).

Tumor grade (in D&C) and MI status (on MRI) were downgraded for 93 cases after surgery. Of these, 20 (6.9%) were downgraded from G2 and G3 to G1/AH, 23 (8.0%) were downgraded from MI to non-MI, 18 (6.3%) were downgraded

from existing CSI to non-CSI, and 32 (11.1%) were downgraded from existing EM to non-EM, respectively. On the contrary, 18 (6.2%) were upgraded from non-MI to MI, 24 (8.3%) and 11 (3.8%) were upgraded from non-CSI and non-EM to CSI and EM according to the final pathology, respectively. The 24 (8.3%) patients were identified as FPT candidates from non-FPT because of an over diagnosis of MI (n=21), CSI (n=2) or LM (n=6) by the radiologists. One case scenario is exhibited in **Figure 2**.

Feature selection and model building

A total of 358 MRI radiomics features were extracted to describe the tumor information, including shape features (n=14), first-order features (n=18×4), and texture features (n=68×4). The 91 features with both the inter- and intra-class ICCs > 0.9 were retained (**Supplementary Table 1**). Thirteen radiomics features (named the radiomics signature), including one Shape_LAL, one shape_M2DDS, and 11 other features for identifying FPT candidates, were selected using LASSO and the radscore formulation was shown in **Supplementary File**. The LASSO selection process for radiomics features, their corresponding coefficients, and the co-occurrence matrix plotting the network of each radiomics feature and clinical information are shown in **Figure 3** and **Supplementary Figure 1**.

Radiomics nomogram in endometrioid carcinoma treatment

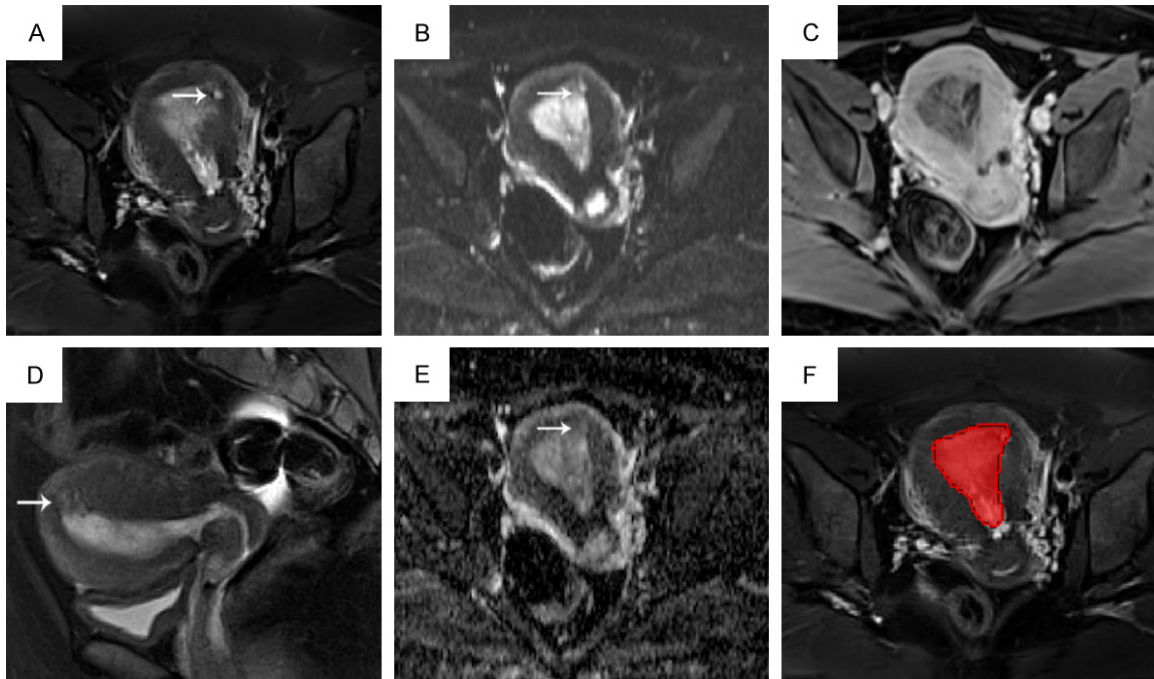


Figure 2. An example of a 36-year-old patient with endometrioid adenocarcinoma and adenomyosis. Superficial myometrial invasion in the left uterine horn region (white arrow) was diagnosed by radiologists but proven to be adenomyosis by surgical pathology. A. Axial T2WI-FS; B. Axial DWI; C. Axial CE-T1WI-FS; D. Sagittal T2WI-FS; E. Axial ADC; F. Region of interest on axial T2WI-FS. ADC, apparent diffusion coefficient; CE-T1WI: contrast-enhanced T1-weighted imaging; DWI, diffusion weighted imaging; FS: fat saturation; T2WI: T2-weighted imaging.

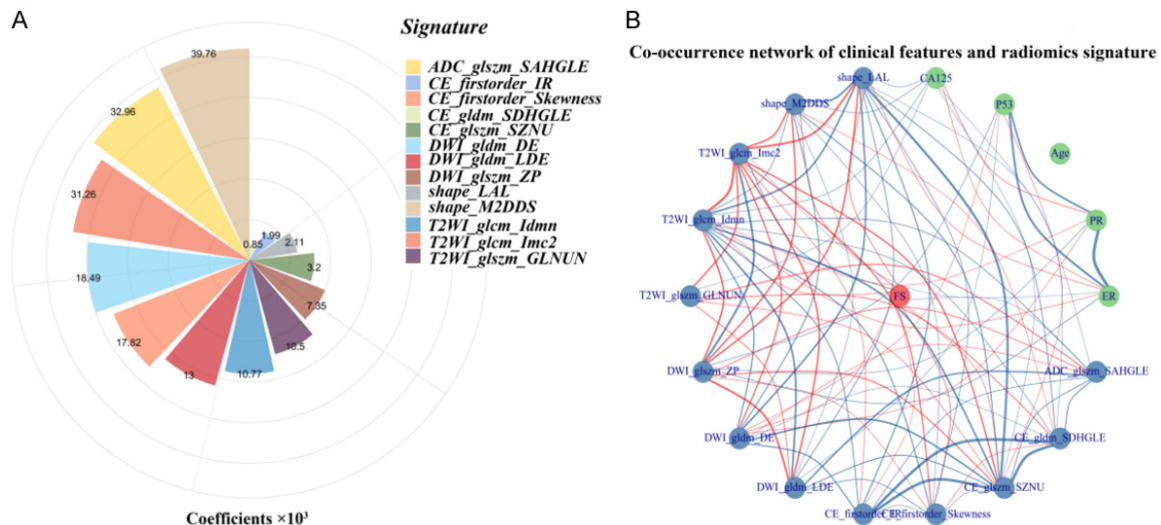


Figure 3. LASSO selection process for radiomics features, the corresponding coefficients and the co-occurrence network of the radiomics features and clinical information. A. The selected features and their corresponding LASSO coefficients, shape_M2DDS has the largest weight; B. The co-occurrence matrix plots the correlations of the patients eligible for FPT (red), clinical information (blue) and radiomics features (green). The blue line indicates a negative correlation, and the red line indicates a positive correlation ($P < 0.05$). FPT: fertility-preserving treatment; LASSO, least absolute shrinkage and selection operator.

The clinical model (combining MI status on MRI and tumor grade from the curettage pathology)

and the radiomics nomogram (integrating the 13 radiomics features with the two clinical fea-

Radiomics nomogram in endometrioid carcinoma treatment

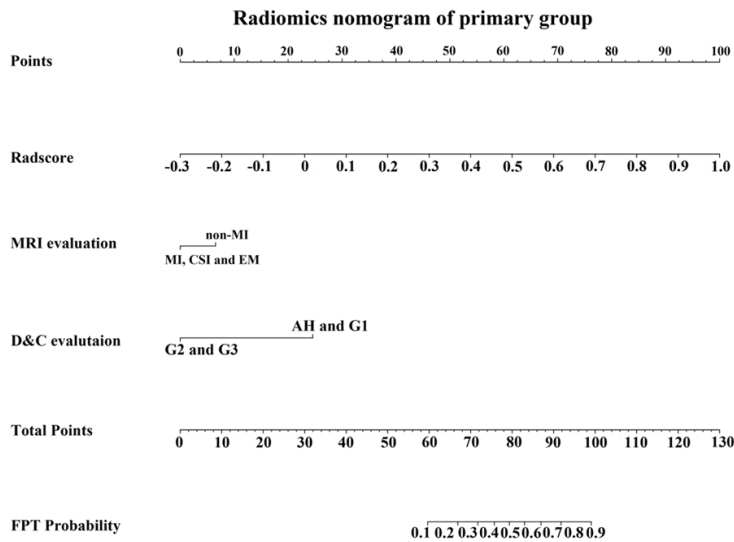


Figure 4. The radiomics nomogram developed. The radiomics nomogram developed from the primary group. Based on this radiomics nomogram, for example, a 30-year-old woman with a radscore of 0.2 (37 points), grade 1 EAC (25 points), and MI (0 points) has a total of 62 points, which corresponds to a probability of FPT eligibility of approximately 13%, resulting in a radiomics nomogram diagnosis of non-FPT. CSI, cervical stromal invasion; D&C, dilatation and curettage; DMI, deep myometrial invasion; EM: extrauterine metastasis; High-grade: G2 and G3; Low-grade: AH and G1; MI, myometrial invasion.

tures) were developed based on the data from the primary group. The developed radiomics nomogram and the calibration curves are shown in **Figures 4** and **5**.

Diagnostic performance assessment

ROC curve analyses, including the AUC, specificity, sensitivity, and accuracy of the clinical model and the radiomics nomogram in the primary group and validation groups 1 and 2 in identifying FPT candidate patients are shown in **Table 3**. The AUCs of radiomics nomogram were 0.86 (95% CI: 0.80-0.93) in the primary group, 0.82 (95% CI: 0.71-0.93) in the validation group 1, and 0.94 (95% CI: 0.87-1.00) in the validation group 2, respectively. DeLong's test showed that the AUC of the radiomics nomogram was higher than that of the clinical model for the three groups (all $P < 0.001$).

With the help of radiomics nomogram, 34 (11.8%) FPT candidates misidentified by the clinical model were changed to non-FPT candidates, and 11 (3.8%) non-FPT candidates misidentified by the clinical model were changed to FPT candidates. CDC analysis showed that if the threshold probability was within 0-1.0, the

radiomics nomogram provided a better net benefit than the treat-all patients scheme or the treat-none scheme, indicating its good clinical usefulness (**Figure 6**). The reclassification measures of discrimination confirmed that the radiomics nomogram performed better than the clinical model based on all the data (including the primary group and validation groups 1 and 2), with an NRI of 0.80 (95% confidence interval [CI]: 0.53-1.07) and an IDI of 0.17 (95% CI: 0.11-0.23) (both $P < 0.05$) (**Figure 7**). This result indicated that for every 100, an additional 17 patients would have an optimal FPT planning assessment using the MRI radiomics nomogram. The NRI and IDI were 0.95 (95% CI: 0.61-1.30) and 0.19 (95% CI: 0.10-0.28) ($P < 0.001$) in primary group, and were 0.65 (95% CI: 0.07-1.22) and 0.08 (95% CI: 0.00-0.17) ($P = 0.03$) in the validation group 1, and were 0.09 (95% CI: -0.03-0.20) and 0.07 (95% CI: -0.09-0.23) ($P = 0.39$) in the validation group 2, respectively.

Discussion

In this study, a radiomics nomogram combining mpMRI radiomics features and clinical information was developed to identify eligible EAC/AH patients for FPT. The radiomics nomogram was also validated with both independent retrospective and prospective data, suggesting its reproducibility and reliability. The radiomics nomogram could aid clinical decision making in selecting eligible FPT patients, especially in helping gynecologists rule out false-negative patients for FPT. NRI and IDI analyses showed the better clinical usefulness of the radiomics nomogram than that of the clinical model for individually identifying eligible EAC/AH patients for receiving FPT.

There have been some reports on FPT using progestins for early-stage EC in young women [4, 18, 21]. The existing important problem in FPT planning is the lack of confidence in the diagnosis of the grade and MI of EC. D&C and endometrial biopsy are two major preoperative examinations that can provide EC grading infor-

Radiomics nomogram in endometrioid carcinoma treatment

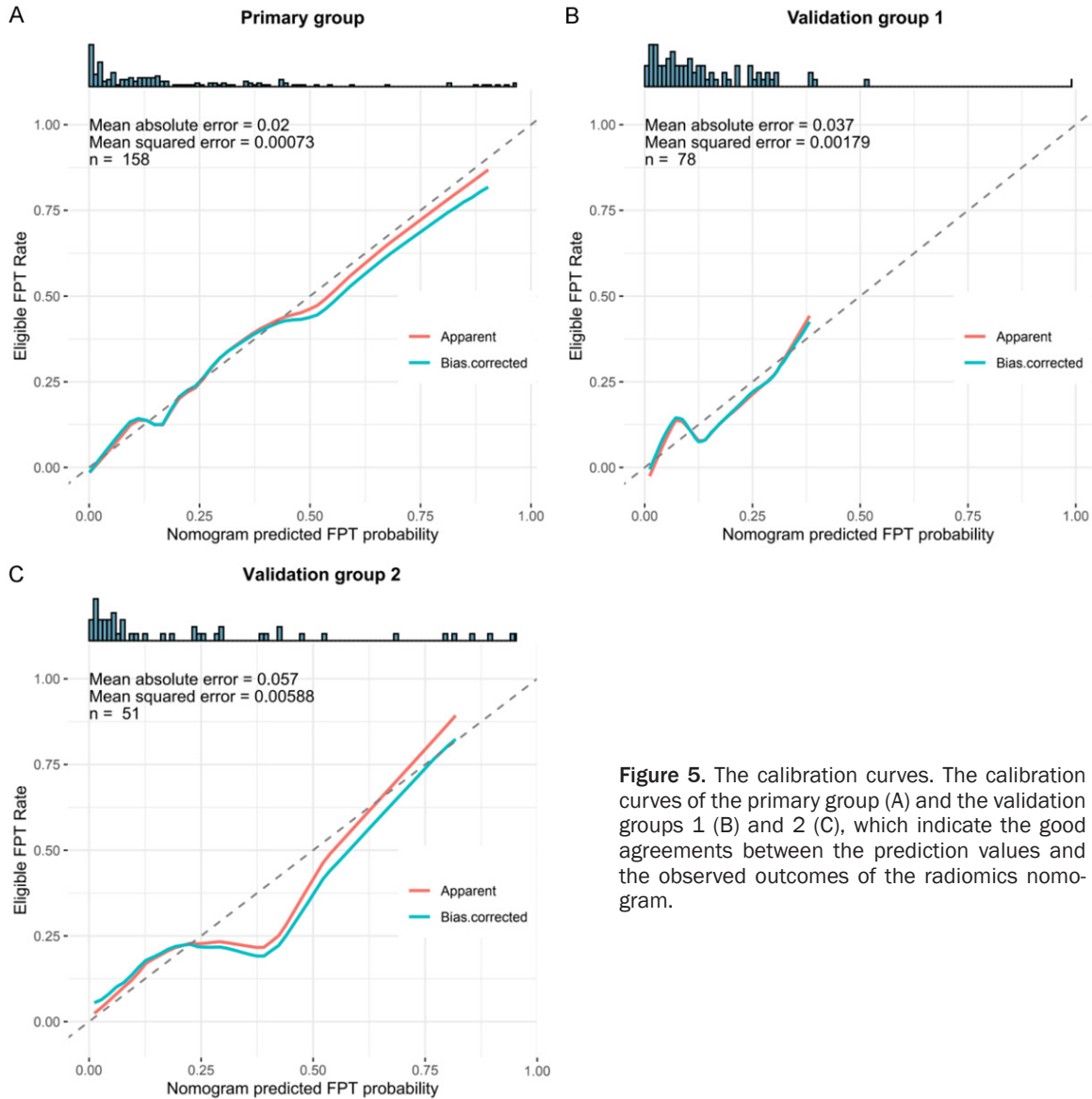


Figure 5. The calibration curves. The calibration curves of the primary group (A) and the validation groups 1 (B) and 2 (C), which indicate the good agreements between the prediction values and the observed outcomes of the radiomics nomogram.

mation. However, studies have shown that there are substantial discrepancies between preoperative and postoperative tumor grading. A study revealed that AH diagnosed by endometrial biopsy coexisted with EC in 42.6% of patients [22]. Others have shown that 14.7-23.2% of biopsies suggested grade I EC, which were upgraded following surgical pathology [5, 7, 23, 24].

It is commonly agreed that the group of patients eligible for FPT is restricted to that with presumed early-stage EC [4, 17, 18, 21]. However, the diagnostic accuracy of imaging for MI has been unsatisfactory. CT scans failed to identify MI in 39% of patients [25]. The accuracy of MRI in detecting MI varies from 68% to 82% with

high false-negative because the signal of the junctional zone on T2WI and subendometrial enhancement on dynamic CE-T1WI are significantly influenced by the periodic cycle [12, 26, 27]. The higher incidence of complicating diseases such as polypoid tumors, adenomyosis, and leiomyoma might be the causes of the lower diagnostic performance of MRI in younger EC patients [28-30]. The lower accuracy of imaging for MI results in difficulty for gynecologists in selecting eligible EC patients for FPT. Thus, the improvement of imaging assessment and rationalization of treatment planning are crucial for young patients with EC.

In the optimization process of the LASSO method for radiomics feature selection, 3 selected

Radiomics nomogram in endometrioid carcinoma treatment

Table 3. Diagnostic performance of the clinical model and the radiomics nomogram in identifying FPT candidate patients

Model	Group	SPE	SEN	ACC	AUC (95% CI)	P value*
Clinical model	Primary	72.6%	53.3%	68.9%	0.63 (0.53-0.73)	
	Validation 1	68.6%	54.5%	66.7%	0.62 (0.45-0.78)	
	Validation 2	85.0%	54.5%	78.4%	0.69 (0.53-0.86)	
Radiomics nomogram	Primary	75.0%	86.7%	77.2%	0.86 (0.80-0.93)	<0.001
	Validation 1	65.7%	90.9%	69.2%	0.82 (0.71-0.93)	0.048
	Validation 2	75.0%	100%	80.3%	0.94 (0.87-1.00)	0.002

*, comparison between clinical model with radiomics nomogram in the primary group and the validation groups. ACC, accuracy; AUC, area under the curve; CI, confidence interval; SEN, sensitivity; SPE, specificity.

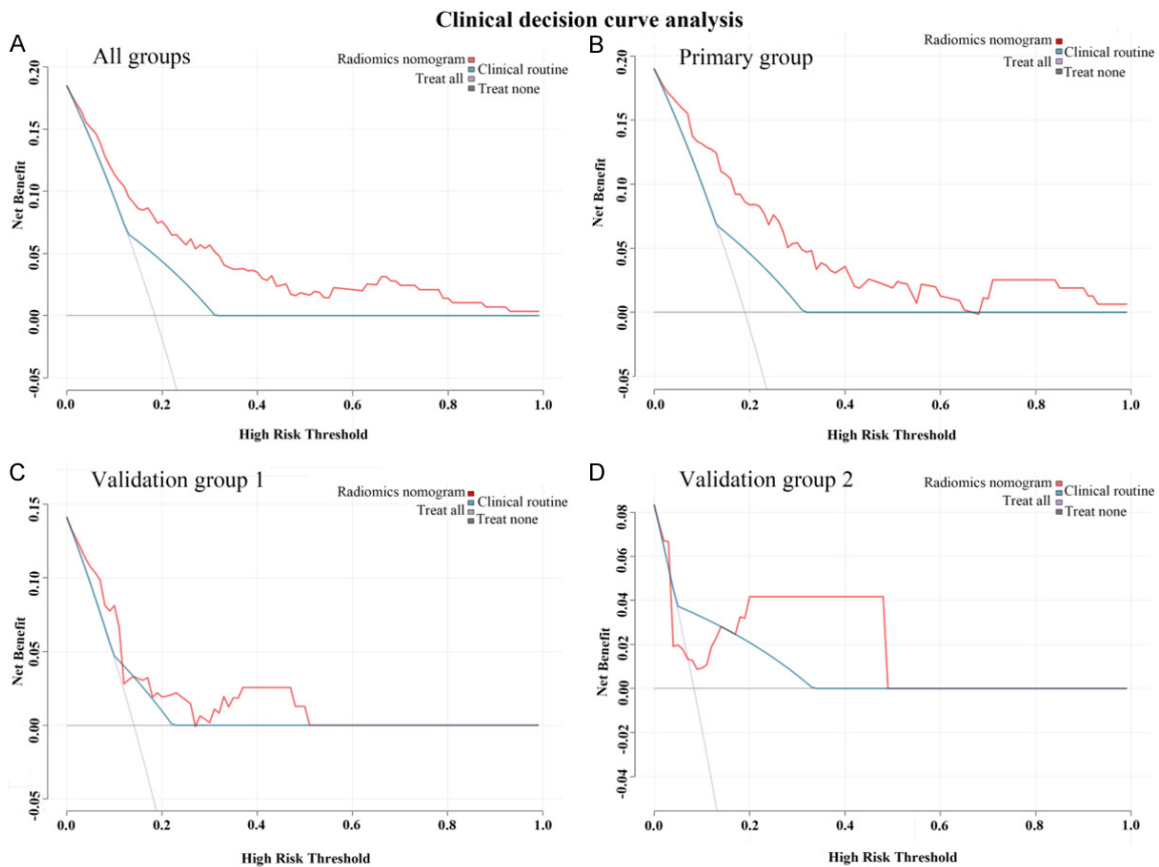


Figure 6. Clinical decision curves for the radiomics nomogram and the clinical model based on primary and validation groups' data. The net benefit is plotted versus the threshold probability that represents the probability of FPT candidates (which is used to trigger a decision to choose that treatment). A-D. They are based on the data of all groups, the primary group, the validation group 1 and the validation group 2, respectively.

features extracted from DWI were important in identifying eligible EAC/AH patients for FPT, which is in accordance with the results for DWI in a systematic review and meta-analysis of EC [31]. CE_Skewness was found to be an important feature for identifying FPT candidates. Similarly, a previous study indicated that CE_Kurtosis was an indicator of MI [32]. Shape_

LAL had high weight among the radiomics features, suggesting an important role of conventional shape-based features in this prediction model. Previous study reported that tumor size was correlated with the grade and MI of EC [33]. Tumor size is commonly used as a prognostic factor in EC patients since it has been correlated with aggressive factors in EC [34].

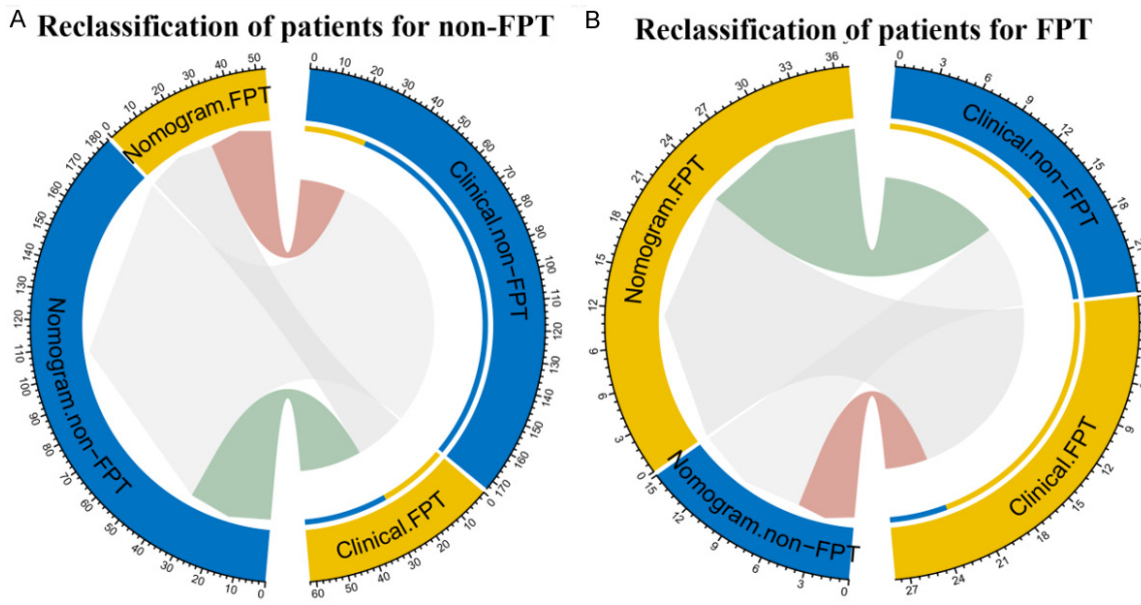


Figure 7. Reclassification of patients for non-FPT (A) and FPT (B) candidates. Groups are illustrated according to the radiomics nomogram and clinical model-determined FPT eligibility basing on the whole dataset with the specific patient numbers presented. The patients are pathological confirmed eligible for non-FPT (A) and FPT (B). In the circle plots, the patients who were classified both correctly by clinical and nomogram are represented as connections in light grey. The connections in light green indicate patients who were diagnosed incorrectly by clinical model but reclassified correctly by the nomogram, while connections in pink indicate patients who were diagnosed correctly by clinical model but reclassified incorrectly by the nomogram.

This study showed that the radiomics nomogram achieved a significantly higher diagnostic performance than the clinical model for all three groups. The radiomics nomogram could concurrently assess the tumor grade and MI, indicating that it is capable of preoperatively identifying eligible EC patients for FPT. It could be a powerful tool for gynecologists to assess the risk probability of FPT and to rule out false-negative EC patients for FPT due to upgrading of the tumor in D&C and overestimation of MI (especially SMI) on MRI. Furthermore, CDC analysis showed that the radiomics nomogram achieved a good net benefit in selecting eligible FPT candidates. The NRI and IDI showed that the application of the radiomics nomogram resulted in approximately 17 of 100 patients benefiting from a precise assessment for FPT eligibility. Therefore, the nomogram could facilitate personalized treatment decisions for EC patients.

Limitations

This study had several limitations. First, many enrolled patients received pelvic MRI after curettage, forcing them to be based on the

residual tumors rather than the intact primary tumors. The curettage procedure might have an influence on MRI findings and DWI parameters. However, the abundant radiomics features might reduce the influence which affected by the D&C procedure. Second, because of the retrospective nature of the data from the primary group, some useful clinical information for selecting FPT, such as body mass index and insulin resistance, were not included, which might have influenced the effectiveness of this nomogram. Third, the various processes used here, from the data processing to the data analysis, model building and generating the diagnosis, could sometimes be time-consuming; however, the higher accuracy and safer treatment decision making for EC patients who hope to receive FPT was a worthwhile trade-off.

Conclusion

This study developed a radiomics nomogram by integrating mpMRI radiomics features with clinical information to identify EAC/AH patients eligible for FPT, with a better performance than the clinical model. The nomogram could be a

useful tool for providing personalized treatment management for EAC/AH patients.

Acknowledgements

We thank for the radiologists who help to our study: Shao Feng DUAN (GE healthcare) gave advice and suggestion on R code and offered some software; Hai Ming LI (Obstetrics and Gynecology Hospital of Fudan University), Lei FU, and Jin Li XING offered great help in patients collection. This study was supported by the National Natural Science Foundation of China (No. 81971579), Shanghai Municipal Health Commission (No. ZK2019B01), Shanghai Municipal Commission of Science and Technology (No. 19411972000).

Disclosure of conflict of interest

None.

Abbreviations

AH, atypical hyperplasia; AUC, the areas under the receiver operating characteristic curve; CDC, clinical decision curve; DMI, deep myometrial invasion; EAC, endometrioid adenocarcinoma; EC, endometrial cancer; FPT, fertility-preserving treatment; IDI, total integrated discrimination index; LASSO, the least absolute shrinkage and selection operator; MI, myometrial invasion; NRI, the net reclassification index; ROIs, regions of interest.

Address correspondence to: Dr. Jin-Wei Qiang, Department of Radiology, Jinshan Hospital, Fudan University, 1508 Longhang Road, Shanghai 201-508, China. Tel: +86-18930819898; E-mail: dr.jinweiqiang@163.com

References

- [1] Morice P, Leary A, Creutzberg C, Abu-Rustum N and Darai E. Endometrial cancer. *Lancet* 2016; 387: 1094-1108.
- [2] Siegel RL, Miller KD and Jemal A. Cancer statistics, 2020. *CA Cancer J Clin* 2020; 70: 7-30.
- [3] Navarria I, Usel M, Rapiti E, Neyroud-Caspar I, Pelte MF, Bouchardy C and Petignat P. Young patients with endometrial cancer: how many could be eligible for fertility-sparing treatment? *Gynecol Oncol* 2009; 114: 448-451.
- [4] Ushijima K, Yahata H, Yoshikawa H, Konishi I, Yasugi T, Saito T, Nakanishi T, Sasaki H, Saji F, Iwasaka T, Hatae M, Kodama S, Saito T, Terakawa N, Yaegashi N, Hiura M, Sakamoto A, Tsuda H, Fukunaga M and Kamura T. Multicenter phase II study of fertility-sparing treatment with medroxyprogesterone acetate for endometrial carcinoma and atypical hyperplasia in young women. *J Clin Oncol* 2007; 25: 2798-2803.
- [5] Nougaret S, Horta M, Sala E, Lakhman Y, Thomassin-Naggara I, Kido A, Masselli G, Bharwani N, Sadowski E, Ertmer A, Otero-Garcia M, Kubik-Huch RA, Cunha TM, Rockall A and Forstner R. Endometrial cancer MRI staging: updated guidelines of the European Society of Urogenital Radiology. *Eur Radiol* 2019; 29: 792-805.
- [6] Batista TP, Cavalcanti CL, Tejo AA and Bezerra AL. Accuracy of preoperative endometrial sampling diagnosis for predicting the final pathology grading in uterine endometrioid carcinoma. *Eur J Surg Oncol* 2016; 42: 1367-1371.
- [7] Eltabbakh GH, Shamonki J and Mount SL. Surgical stage, final grade, and survival of women with endometrial carcinoma whose preoperative endometrial biopsy shows well-differentiated tumors. *Gynecol Oncol* 2005; 99: 309-312.
- [8] Helpman L, Kupets R, Covens A, Saad RS, Khalifa MA, Ismiil N, Ghorab Z, Dubé V and Nofech-Mozes S. Assessment of endometrial sampling as a predictor of final surgical pathology in endometrial cancer. *Br J Cancer* 2014; 110: 609-615.
- [9] Suh DS, Kim JK, Kim KR, Kim DY, Kim JH, Kim YM, Kim YT and Nam JH. Reliability of magnetic resonance imaging in assessing myometrial invasion absence in endometrial carcinoma. *Acta Obstet Gynecol Scand* 2009; 88: 990-993.
- [10] Nakao Y, Yokoyama M, Hara K, Koyamatsu Y, Yasunaga M, Araki Y, Watanabe Y and Iwasaka T. MR imaging in endometrial carcinoma as a diagnostic tool for the absence of myometrial invasion. *Gynecol Oncol* 2006; 102: 343-347.
- [11] Lin G, Ng KK, Chang CJ, Wang JJ, Ho KC, Yen TC, Wu TI, Wang CC, Chen YR, Huang YT, Ng SH, Jung SM, Chang TC and Lai CH. Myometrial invasion in endometrial cancer: diagnostic accuracy of diffusion-weighted 3.0-T MR imaging-initial experience. *Radiology* 2009; 250: 784-792.
- [12] Cade TJ, Quinn MA, McNally OM, Neesham D, Pyman J and Dobrotwir A. Predictive value of magnetic resonance imaging in assessing myometrial invasion in endometrial cancer: is radiological staging sufficient for planning conservative treatment? *Int J Gynecol Cancer* 2010; 20: 1166-1169.
- [13] Sakane M, Hori M, Onishi H, Tsuboyama T, Ota T, Tatsumi M, Ueda Y, Kimura T, Kimura T and Tomiyama N. Assessment of myometrial inva-

Radiomics nomogram in endometrioid carcinoma treatment

- sion in premenopausal grade 1 endometrial carcinoma: is magnetic resonance imaging a reliable tool in selecting patients for fertility-preserving therapy? *J Comput Assist Tomogr* 2018; 42: 412-417.
- [14] Park JJ, Kim CK, Cho SW and Kim JH. Utility of diffusion-weighted imaging in association with pathologic upgrading in biopsy-proven grade I endometrial cancer. *J Magn Reson Imaging* 2020; 51: 117-123.
- [15] Balachandran VP, Gonen M, Smith JJ and DeMatteo RP. Nomograms in oncology: more than meets the eye. *Lancet Oncol* 2015; 16: e173-e180.
- [16] Pan YX, Chen JC, Fang AP, Wang XH, Chen JB, Wang JC, He W, Fu YZ, Xu L, Chen MS, Zhang YJ, Li QJ and Zhou ZG. A nomogram predicting the recurrence of hepatocellular carcinoma in patients after laparoscopic hepatectomy. *Cancer Commun (Lond)* 2019; 39: 55.
- [17] Koh WJ, Abu-Rustum NR, Bean S, Bradley K, Campos SM, Cho KR, Chon HS, Chu C, Cohn D, Crispens MA, Damast S, Dorigo O, Eifel PJ, Fisher CM, Frederick P, Gaffney DK, George S, Han E, Higgins S, Huh WK, Lurain JR 3rd, Mariani A, Mutch D, Nagel C, Nekhlyudov L, Fader AN, Remmenga SW, Reynolds RK, Tillmanns T, Ueda S, Wyse E, Yashar CM, McMillian NR and Scavone JL. Uterine neoplasms, version 1.2018, NCCN clinical practice guidelines in oncology. *J Natl Compr Canc Netw* 2018; 16: 170-199.
- [18] Zhou S, Xu Z, Yang B, Guan J, Shan W, Shi Y and Chen X. Characteristics of progestin-insensitive early stage endometrial cancer and atypical hyperplasia patients receiving second-line fertility-sparing treatment. *J Gynecol Oncol* 2021; 32: e57.
- [19] Sala E, Rockall AG, Freeman SJ, Mitchell DG and Reinhold C. The added role of MR imaging in treatment stratification of patients with gynecologic malignancies: what the radiologist needs to know. *Radiology* 2013; 266: 717-740.
- [20] Tibshirani R. Regression shrinkage and selection via the lasso. *J R Stat Soc Ser B* 1996; 58: 267-288.
- [21] Kaku T, Yoshikawa H, Tsuda H, Sakamoto A, Fukunaga M, Kuwabara Y, Hataeg M, Kodama S, Kuzuya K, Sato S, Nishimura T, Hiura M, Nakano H, Iwasaka T, Miyazaki K and Kamura T. Conservative therapy for adenocarcinoma and atypical endometrial hyperplasia of the endometrium in young women: central pathologic review and treatment outcome. *Cancer Lett* 2001; 167: 39-48.
- [22] Trimble CL, Kauderer J, Zaino R, Silverberg S, Lim PC, Burke JJ 2nd, Alberts D and Curtin J. Concurrent endometrial carcinoma in women with a biopsy diagnosis of atypical endometrial hyperplasia: a gynecologic oncology group study. *Cancer* 2006; 106: 812-819.
- [23] Frumovitz M, Singh DK, Meyer L, Smith DH, Wertheim I, Resnik E and Bodurka DC. Predictors of final histology in patients with endometrial cancer. *Gynecol Oncol* 2004; 95: 463-468.
- [24] Leitao MM Jr, Kehoe S, Barakat RR, Alektiar K, Gattoc LP, Rabbitt C, Chi DS, Soslow RA and Abu-Rustum NR. Accuracy of preoperative endometrial sampling diagnosis of FIGO grade 1 endometrial adenocarcinoma. *Gynecol Oncol* 2008; 111: 244-248.
- [25] Zerbe MJ, Bristow R, Grumbine FC and Montz FJ. Inability of preoperative computed tomography scans to accurately predict the extent of myometrial invasion and extracorporeal spread in endometrial cancer. *Gynecol Oncol* 2000; 78: 67-70.
- [26] Ben-Shachar I, Vitellas KM and Chon DE. The role of MRI in the conservative management of endometrial cancer. *Gynecol Oncol* 2004; 93: 233-237.
- [27] Kido A, Koyama T, Kataoka M, Yamamoto A, Saga T, Turner R and Togashi K. Physiological changes of the human uterine myometrium during menstrual cycle: preliminary evaluation using BOLD MR imaging. *J Magn Reson Imaging* 2007; 26: 695-700.
- [28] Hori M, Kim T, Murakami T, Imaoka I, Onishi H, Nakamoto A, Nakaya Y, Tomoda K, Tsutsui T, Enomoto T, Kimura T and Nakamura H. MR imaging of endometrial carcinoma for preoperative staging at 3.0 T: comparison with imaging at 1.5 T. *J Magn Reson Imaging* 2009; 30: 621-630.
- [29] Kaneda S, Fujii S, Fukunaga T, Kakite S, Kaminou T, Kigawa J, Harada T and Ogawa T. Myometrial invasion by endometrial carcinoma: evaluation with 3.0T MR imaging. *Abdom Imaging* 2011; 36: 612-618.
- [30] Foti PV, Farina R, Coronella M, Ruggeri C, Palmucci S, Montana A, Milone P, Zarbo G, Caltabiano R, Lanzafame S, Politi G and Ettorre GC. Endometrial carcinoma: MR staging and causes of error. *Radiol Med* 2013; 118: 487-503.
- [31] Andreano A, Rechichi G, Rebora P, Sironi S, Valsecchi MG and Galimberti S. MR diffusion imaging for preoperative staging of myometrial invasion in patients with endometrial cancer: a systematic review and meta-analysis. *Eur Radiol* 2014; 24: 1327-1338.
- [32] Ytre-Hauge S, Dybvik JA, Lundervold A, Salvesen ØO, Krakstad C, Fasmer KE, Werner HM, Ganeshan B, Høivik E, Bjørge L, Trovik J and Haldorsen IS. Preoperative tumor texture analysis on MRI predicts high-risk disease and reduced survival in endometrial cancer. *J Magn Reson Imaging* 2018; 48: 1637-1647.

Radiomics nomogram in endometrioid carcinoma treatment

- [33] Nougaret S, Reinhold C, Alsharif SS, Addley H, Arceneau J, Molinari N, Guiu B and Sala E. Endometrial cancer: combined MR volumetry and diffusion-weighted imaging for assessment of myometrial and lymphovascular invasion and tumor grade. *Radiology* 2015; 276: 797-808.
- [34] Berretta R, Patrelli TS, Migliavacca C, Rolla M, Franchi L, Monica M, Modena AB and Gizzo S. Assessment of tumor size as a useful marker for the surgical staging of endometrial cancer. *Oncol Rep* 2014; 31: 2407-2412.

Radiomics nomogram in endometrioid carcinoma treatment

Supplementary File

The formulation of radscore: $\text{Radscore} = 0.18987 + -0.02802 \times \text{shape_LAL} + -0.08874 \times \text{shape_M2DDS} + 0.04418 \times \text{T2WI_glcm_lmc2} + -0.05692 \times \text{T2WI_glcm_ldmn} + -0.02245 \times \text{T2WI_glszm_GLNUN} + -0.05061 \times \text{DWI_glszm_ZP} + 0.01202 \times \text{DWI_gldm_DE} + 0.06208 \times \text{DWI_gldm_LDE} + -0.00824 \times \text{CE_firstorder_IR} + -0.04121 \times \text{CE_firstorder_Skewness} + -0.01104 \times \text{CE_glszm_SZNU} + -0.03293 \times \text{CE_gldm_SDHGLE} + 0.10102 \times \text{ADC_glszm_SAHGLE}$.

Supplementary Table 1. The inter- and intra-class correlation coefficients (ICCs) of 385 radiomics features

Radiomics features	Intra-class ICC	Inter-class ICC
shape_Elongation	0.61	0.88
shape_Flatness	0.46	0.93
shape_LAL	0.84	0.96
shape_MAL	0.82	0.96
shape_M2DDC	0.90	0.97
shape_M2DDR	0.81	0.95
shape_M2DDS	0.95	0.96
shape_M3DD	0.83	0.95
shape_MeshVolume	0.92	0.99
shape_MinorAxisLength	0.76	0.93
shape_Sphericity	0.57	0.74
shape_SurfaceArea	0.89	0.98
shape_SurfaceVolumeRatio	0.75	0.87
shape_VoxelVolume	0.92	0.99
T2WI_firstorder_10P	0.79	0.79
T2WI_firstorder_90P	0.90	0.87
T2WI_firstorder_Energy	0.99	1.00
T2WI_firstorder_Entropy	0.83	0.94
T2WI_firstorder_IR	0.81	0.94
T2WI_firstorder_Kurtosis	0.71	0.51
T2WI_firstorder_Maximum	0.81	0.66
T2WI_firstorder_MAD	0.82	0.93
T2WI_firstorder_Mean	0.90	0.86
T2WI_firstorder_Median	0.89	0.90
T2WI_firstorder_Minimum	0.57	0.37
T2WI_firstorder_Range	0.75	0.71
T2WI_firstorder_RobustMAD	0.81	0.94
T2WI_firstorder_RootMeanSquared	0.90	0.87
T2WI_firstorder_Skewness	0.67	0.58
T2WI_firstorder_TotalEnergy	0.95	1.00
T2WI_firstorder_Uniformity	0.76	0.96
T2WI_firstorder_Variance	0.75	0.91
T2WI_glcm_Autocorrelation	0.80	0.81
T2WI_glcm_JointAverage	0.76	0.82
T2WI_glcm_CP	0.44	0.88
T2WI_glcm_ClusterShade	0.70	0.72
T2WI_glcm_ClusterTendency	0.67	0.87
T2WI_glcm_Contrast	0.84	0.90
T2WI_glcm_Correlation	0.75	0.84

Radiomics nomogram in endometrioid carcinoma treatment

T2WI_glcm_DifferenceAverage	0.89	0.92
T2WI_glcm_DE	0.88	0.92
T2WI_glcm_DV	0.80	0.83
T2WI_glcm_JointEnergy	0.64	0.92
T2WI_glcm_JointEntropy	0.84	0.89
T2WI_glcm_Imc1	0.86	0.79
T2WI_glcm_Imc2	0.88	0.91
T2WI_glcm_Idm	0.91	0.95
T2WI_glcm_Idmn	0.80	0.84
T2WI_glcm_Id	0.91	0.95
T2WI_glcm_Idn	0.85	0.86
T2WI_glcm_InverseVariance	0.91	0.95
T2WI_glcm_MaximumProbability	0.59	0.95
T2WI_glcm_SumEntropy	0.82	0.90
T2WI_glcm_SumSquares	0.73	0.89
T2WI_glrIm_GLNU	0.96	1.00
T2WI_glrIm_GLNUN	0.77	0.95
T2WI_glrIm_GLV	0.75	0.91
T2WI_glrIm_HGLRE	0.82	0.81
T2WI_glrIm_LongRunEmphasis	0.94	0.99
T2WI_glrIm_LRHGLE	0.81	0.82
T2WI_glrIm_LRLGLE	0.55	0.67
T2WI_glrIm_LGLRE	0.55	0.64
T2WI_glrIm_RunEntropy	0.79	0.92
T2WI_glrIm_RLNU	0.97	0.99
T2WI_glrIm_RLNUN	0.92	0.95
T2WI_glrIm_RunPercentage	0.92	0.96
T2WI_glrIm_RunVariance	0.95	0.99
T2WI_glrIm_SRE	0.92	0.96
T2WI_glrIm_SRHGLE	0.83	0.81
T2WI_glrIm_SRLGLE	0.55	0.63
T2WI_glszm_GLNU	0.94	0.99
T2WI_glszm_GLNUN	0.76	0.91
T2WI_glszm_GLV	0.74	0.83
T2WI_glszm_HGLZE	0.80	0.77
T2WI_glszm_LAE	0.98	0.99
T2WI_glszm_LAHGLE	0.96	0.96
T2WI_glszm_LALGLE	0.87	0.87
T2WI_glszm_LGLZE	0.53	0.70
T2WI_glszm_SZNU	0.94	0.98
T2WI_glszm_SZNUN	0.86	0.87
T2WI_glszm_SAE	0.84	0.87
T2WI_glszm_SAHGLE	0.84	0.75
T2WI_glszm_SALGLE	0.52	0.69
T2WI_glszm_ZoneEntropy	0.81	0.89
T2WI_glszm_ZP	0.89	0.92
T2WI_glszm_ZoneVariance	0.98	0.99
T2WI_gldm_DE	0.82	0.88
T2WI_gldm_DNU	0.96	0.99
T2WI_gldm_DNUN	0.91	0.93

Radiomics nomogram in endometrioid carcinoma treatment

T2WI_gldm_DependenceVariance	0.91	0.98
T2WI_gldm_GLNU	0.96	1.00
T2WI_gldm_GLV	0.75	0.91
T2WI_gldm_HGLE	0.82	0.81
T2WI_gldm_LDE	0.93	0.98
T2WI_gldm_LargeDependenceHGLE	0.86	0.86
T2WI_gldm_LDLGE	0.63	0.85
T2WI_gldm_LGLEG	0.55	0.63
T2WI_gldm_SDE	0.89	0.91
T2WI_gldm_SDHGLE	0.93	0.81
T2WI_gldm_SDLGLEG	0.64	0.63
DWI_firstorder_10P	0.92	0.94
DWI_firstorder_90P	0.99	0.98
DWI_firstorder_Energy	1.00	1.00
DWI_firstorder_Entropy	0.89	0.96
DWI_firstorder_IR	0.96	0.98
DWI_firstorder_Kurtosis	0.66	0.80
DWI_firstorder_Maximum	0.97	0.99
DWI_firstorder_MAD	0.97	0.99
DWI_firstorder_Mean	0.97	0.98
DWI_firstorder_Median	0.96	0.98
DWI_firstorder_Minimum	0.75	0.80
DWI_firstorder_Range	0.95	0.98
DWI_firstorder_RobustMAD	0.96	0.98
DWI_firstorder_RootMeanSquared	0.98	0.98
DWI_firstorder_Skewness	0.67	0.94
DWI_firstorder_TotalEnergy	0.99	1.00
DWI_firstorder_Uniformity	0.74	0.95
DWI_firstorder_Variance	0.99	1.00
DWI_glcm_Autocorrelation	0.98	0.98
DWI_glcm_JointAverage	0.94	0.96
DWI_glcm_CP	0.98	0.99
DWI_glcm_ClusterShade	0.95	1.00
DWI_glcm_ClusterTendency	0.97	0.99
DWI_glcm_Contrast	0.92	0.97
DWI_glcm_Correlation	0.72	0.56
DWI_glcm_DifferenceAverage	0.85	0.89
DWI_glcm_DE	0.88	0.95
DWI_glcm_DV	0.95	0.99
DWI_glcm_JointEnergy	0.76	0.97
DWI_glcm_JointEntropy	0.90	0.97
DWI_glcm_Imc1	0.57	0.48
DWI_glcm_Imc2	0.65	0.83
DWI_glcm_Idm	0.82	0.84
DWI_glcm_Idmn	0.67	0.32
DWI_glcm_Id	0.81	0.82
DWI_glcm_Idn	0.69	0.47
DWI_glcm_InverseVariance	0.76	0.71
DWI_glcm_MaximumProbability	0.77	0.97

Radiomics nomogram in endometrioid carcinoma treatment

DWI_glcm_SumEntropy	0.89	0.94
DWI_glcm_SumSquares	0.98	0.99
DWI_glrm_GLNU	0.94	0.99
DWI_glrm_GLNUN	0.81	0.92
DWI_glrm_GLV	0.99	0.99
DWI_glrm_HGLRE	0.98	0.98
DWI_glrm_LongRunEmphasis	0.90	0.98
DWI_glrm_LRHGLE	0.99	1.00
DWI_glrm_LRLGLE	0.76	0.97
DWI_glrm_LGLRE	0.78	0.87
DWI_glrm_RunEntropy	0.88	0.87
DWI_glrm_RLNU	0.98	0.99
DWI_glrm_RLNUN	0.80	0.79
DWI_glrm_RunPercentage	0.84	0.89
DWI_glrm_RunVariance	0.94	0.99
DWI_glrm_SRE	0.72	0.89
DWI_glrm_SRHGLE	0.98	0.98
DWI_glrm_SRLGLE	0.70	0.83
DWI_glszm_GLNU	0.69	0.92
DWI_glszm_GLNUN	0.69	0.92
DWI_glszm_GLV	0.92	0.96
DWI_glszm_HGLZE	0.94	0.98
DWI_glszm_LAE	0.94	0.99
DWI_glszm_LAHGLE	0.99	1.00
DWI_glszm_LALGLE	0.70	0.96
DWI_glszm_LGLZE	0.74	0.88
DWI_glszm_SZNU	0.62	0.87
DWI_glszm_SZNUN	0.51	0.80
DWI_glszm_SAE	0.22	0.69
DWI_glszm_SAHGLE	0.61	0.75
DWI_glszm_SALGLE	0.14	0.72
DWI_glszm_ZoneEntropy	0.84	0.89
DWI_glszm_ZP	0.75	0.88
DWI_glszm_ZoneVariance	0.95	0.99
DWI_gldm_DE	0.90	0.80
DWI_gldm_DNU	0.99	0.99
DWI_gldm_DNUN	0.79	0.61
DWI_gldm_DependenceVariance	0.87	0.89
DWI_gldm_GLNU	0.95	0.99
DWI_gldm_GLV	0.99	0.99
DWI_gldm_HGLE	0.98	0.98
DWI_gldm_LDE	0.86	0.92
DWI_gldm_LargeDependenceHGLE	0.97	0.99
DWI_gldm_LDLGLE	0.79	0.85
DWI_gldm_LGLEG	0.76	0.84
DWI_gldm_SDE	0.65	0.86
DWI_gldm_SDHGLE	0.94	0.96
DWI_gldm_SDLGLEG	0.49	0.88
CE_firstorder_10P	0.84	0.87

Radiomics nomogram in endometrioid carcinoma treatment

CE_firstorder_90P	0.86	0.86
CE_firstorder_Energy	0.95	0.99
CE_firstorder_Entropy	0.82	0.92
CE_firstorder_IR	0.79	0.96
CE_firstorder_Kurtosis	0.47	0.76
CE_firstorder_Maximum	0.88	0.88
CE_firstorder_MAD	0.80	0.94
CE_firstorder_Mean	0.87	0.84
CE_firstorder_Median	0.87	0.83
CE_firstorder_Minimum	0.89	0.92
CE_firstorder_Range	0.87	0.97
CE_firstorder_RobustMAD	0.79	0.95
CE_firstorder_RootMeanSquared	0.87	0.84
CE_firstorder_Skewness	0.88	0.81
CE_firstorder_TotalEnergy	0.90	0.99
CE_firstorder_Uniformity	0.75	0.88
CE_firstorder_Variance	0.85	0.97
CE_glcM_Autocorrelation	0.83	0.97
CE_glcM_JointAverage	0.83	0.96
CE_glcM_CP	0.83	0.96
CE_glcM_ClusterShade	0.67	0.93
CE_glcM_ClusterTendency	0.77	0.95
CE_glcM_Contrast	0.85	0.85
CE_glcM_Correlation	0.73	0.73
CE_glcM_DifferenceAverage	0.82	0.75
CE_glcM_DE	0.83	0.94
CE_glcM_DV	0.87	0.98
CE_glcM_JointEnergy	0.69	0.91
CE_glcM_JointEntropy	0.85	0.97
CE_glcM_Imc1	0.55	0.42
CE_glcM_Imc2	0.64	0.74
CE_glcM_Idm	0.78	0.75
CE_glcM_Idmn	0.89	0.29
CE_glcM_Id	0.79	0.75
CE_glcM_Idn	0.86	0.45
CE_glcM_InverseVariance	0.68	0.62
CE_glcM_MaximumProbability	0.76	0.92
CE_glcM_SumEntropy	0.80	0.97
CE_glcM_SumSquares	0.81	0.94
CE_glrIm_GLNU	0.97	0.99
CE_glrIm_GLNUN	0.74	0.88
CE_glrIm_GLV	0.86	0.97
CE_glrIm_HGLRE	0.86	0.97
CE_glrIm_LongRunEmphasis	0.89	0.94
CE_glrIm_LRHGLE	0.87	0.93
CE_glrIm_LRLGLE	0.57	0.94
CE_glrIm_LGLRE	0.46	0.93
CE_glrIm_RunEntropy	0.81	0.97
CE_glrIm_RLNU	0.95	1.00

Radiomics nomogram in endometrioid carcinoma treatment

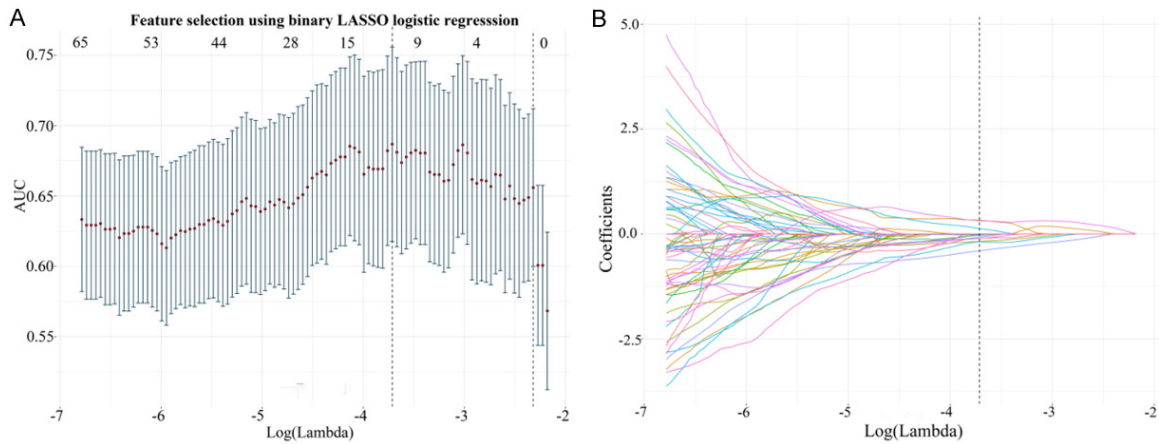
CE_glrIm_RLNUN	0.88	0.85
CE_glrIm_RunPercentage	0.89	0.87
CE_glrIm_RunVariance	0.88	0.95
CE_glrIm_SRE	0.90	0.87
CE_glrIm_SRHGLE	0.87	0.97
CE_glrIm_SRLGLE	0.42	0.93
CE_glszm_GLNU	0.92	0.99
CE_glszm_GLNUN	0.75	0.90
CE_glszm_GLV	0.87	0.97
CE_glszm_HGLZE	0.89	0.97
CE_glszm_LAE	0.97	0.97
CE_glszm_LAHGLE	0.99	0.96
CE_glszm_LALGLE	0.94	0.98
CE_glszm_LGLZE	0.32	0.79
CE_glszm_SZNU	0.90	0.99
CE_glszm_SZNUN	0.63	0.79
CE_glszm_SAE	0.66	0.81
CE_glszm_SAHGLE	0.90	0.97
CE_glszm_SALGLE	0.21	0.65
CE_glszm_ZoneEntropy	0.84	0.97
CE_glszm_ZP	0.72	0.79
CE_glszm_ZoneVariance	0.97	0.97
CE_gldm_DE	0.89	0.96
CE_gldm_DNU	0.94	1.00
CE_gldm_DNUN	0.78	0.82
CE_gldm_DependenceVariance	0.89	0.92
CE_gldm_GLNU	0.98	0.99
CE_gldm_GLV	0.85	0.97
CE_gldm_HGLE	0.86	0.97
CE_gldm_LDE	0.91	0.91
CE_gldm_LargeDependenceHGLE	0.78	0.89
CE_gldm_LDLGE	0.71	0.93
CE_gldm_LGLEG	0.47	0.93
CE_gldm_SDE	0.71	0.79
CE_gldm_SDHGLE	0.89	0.97
CE_gldm_SDLGLEG	0.61	0.88
ADC_firstorder_10P	0.80	0.97
ADC_firstorder_90P	0.86	0.95
ADC_firstorder_Energy	0.93	0.99
ADC_firstorder_Entropy	0.55	0.94
ADC_firstorder_IR	0.72	0.94
ADC_firstorder_Kurtosis	0.46	0.95
ADC_firstorder_Maximum	0.75	0.87
ADC_firstorder_MAD	0.69	0.96
ADC_firstorder_Mean	0.84	0.96
ADC_firstorder_Median	0.79	0.97
ADC_firstorder_Minimum	0.84	0.87
ADC_firstorder_Range	0.76	0.87
ADC_firstorder_RobustMAD	0.70	0.96

Radiomics nomogram in endometrioid carcinoma treatment

ADC_firstorder_RootMeanSquared	0.90	0.95
ADC_firstorder_Skewness	0.71	0.96
ADC_firstorder_TotalEnergy	0.84	0.98
ADC_firstorder_Uniformity	0.02	1.00
ADC_firstorder_Variance	0.71	0.96
ADC_glcmm_Autocorrelation	0.61	0.78
ADC_glcmm_JointAverage	0.59	0.81
ADC_glcmm_CP	0.53	0.93
ADC_glcmm_ClusterShade	0.33	0.96
ADC_glcmm_ClusterTendency	0.66	0.94
ADC_glcmm_Contrast	0.79	0.97
ADC_glcmm_Correlation	0.55	0.82
ADC_glcmm_DifferenceAverage	0.80	0.98
ADC_glcmm_DE	0.78	0.91
ADC_glcmm_DV	0.56	0.96
ADC_glcmm_JointEnergy	0.0	0.99
ADC_glcmm_JointEntropy	0.67	0.84
ADC_glcmm_Imc1	0.88	0.89
ADC_glcmm_Imc2	0.87	0.99
ADC_glcmm_Idm	0.61	0.99
ADC_glcmm_Idmn	0.57	0.83
ADC_glcmm_Id	0.66	0.99
ADC_glcmm_Idn	0.74	0.85
ADC_glcmm_InverseVariance	0.85	0.98
ADC_glcmm_MaximumProbability	0.02	1.00
ADC_glcmm_SumEntropy	0.67	0.79
ADC_glcmm_SumSquares	0.72	0.96
ADC_glrmm_GLNU	0.99	1.00
ADC_glrmm_GLNUN	0.16	0.98
ADC_glrmm_GLV	0.66	0.97
ADC_glrmm_HGLRE	0.72	0.82
ADC_glrmm_LongRunEmphasis	0.35	1.00
ADC_glrmm_LRHGLE	0.69	0.80
ADC_glrmm_LRLGLE	0.01	1.00
ADC_glrmm_LGLRE	0.02	0.99
ADC_glrmm_RunEntropy	0.71	0.89
ADC_glrmm_RLNU	0.95	0.99
ADC_glrmm_RLNUN	0.61	0.99
ADC_glrmm_RunPercentage	0.43	1.00
ADC_glrmm_RunVariance	0.31	1.00
ADC_glrmm_SRE	0.57	0.99
ADC_glrmm_SRHGLE	0.72	0.83
ADC_glrmm_SRLGLE	0.01	0.98
ADC_glszm_GLNU	0.86	0.99
ADC_glszm_GLNUN	0.71	0.92
ADC_glszm_GLV	0.69	0.96
ADC_glszm_HGLZE	0.73	0.82
ADC_glszm_LAE	0.89	0.99
ADC_glszm_LAHGLE	0.80	1.00

Radiomics nomogram in endometrioid carcinoma treatment

ADC_glszm_LALGLE	0.0	0.96
ADC_glszm_LGLZE	0.39	0.62
ADC_glszm_SZNU	0.81	0.97
ADC_glszm_SZNUN	0.91	0.90
ADC_glszm_SAE	0.91	0.92
ADC_glszm_SAHGLE	0.78	0.86
ADC_glszm_SALGLE	0.52	0.54
ADC_glszm_ZoneEntropy	0.87	0.85
ADC_glszm_ZP	0.92	0.97
ADC_glszm_ZoneVariance	0.89	0.99
ADC_gldm_DE	0.86	0.84
ADC_gldm_DNU	0.87	0.98
ADC_gldm_DNUN	0.90	0.91
ADC_gldm_DependenceVariance	0.03	1.00
ADC_gldm_GLNU	0.97	1.00
ADC_gldm_GLV	0.71	0.96
ADC_gldm_HGLE	0.70	0.82
ADC_gldm_LDE	0.10	1.00
ADC_gldm_LargeDependenceHGLE	0.66	0.69
ADC_gldm_LDLGE	0.0	1.00
ADC_gldm_LGLE	0.02	1.00
ADC_gldm_SDE	0.92	0.94
ADC_gldm_SDHGLE	0.81	0.91
ADC_gldm_SDLGLE	0.62	0.50



Supplementary Figure 1. LASSO selection process for radiomics features. A. Selection of the tuning parameter lambda (λ) using 10-fold cross-validation. Binomial deviances from the LASSO regression cross-validation model are plotted as a function of log (λ); B. LASSO coefficient profiles of the 13 radiomics features.